

Mechanical properties of directionally solidified $\text{Al}_2\text{O}_3\text{--ZrO}_2(\text{Y}_2\text{O}_3)$ eutectics

J.Y. Pastor ^a, P. Poza ^a, J. LLorca ^{a,*}, J.I. Peña ^b, R.I. Merino ^b, V.M. Orera ^b

^a *Department of Materials Science, Polytechnic University of Madrid, E.T.S. de Ingenieros de Caminos, 28040 Madrid, Spain*

^b *Instituto de Ciencia de Materiales de Aragón, C.S.I.C., Universidad de Zaragoza. 50009 Zaragoza, Spain*

Received 4 August 2000; received in revised form 9 October 2000

Abstract

The relationship between microstructure and mechanical properties was studied in $\text{Al}_2\text{O}_3\text{--ZrO}_2$ eutectic rods. The material, produced by directional solidification using the laser-heated float zone method, was formed mainly of colonies consisting of a fine interpenetrating or ordered network of ZrO_2 and $\alpha\text{-Al}_2\text{O}_3$ surrounded by a thick boundary region that contained pores and other defects. The flexure strength of the eutectic rods was excellent (> 1.1 GPa) owing to the small critical defect size and the high toughness (7.8 MPa \sqrt{m}). No microstructural changes were observed after about 1 h of exposure at 1700 K, and the eutectic oxide maintained a very high strength up to this temperature. The nature of the critical defects that led to fracture, the toughening micromechanisms, and the differences between the longitudinal and transverse strength are discussed in the light of the microstructural features of the material. © 2001 Elsevier Science B.V. All rights reserved.

Keywords: Directional solidification; Eutectic oxides; High temperature; Mechanical properties

1. Introduction

It is well established that phase distribution, size, and shape as well as interface characteristics play a crucial role in determining the behavior of multiphase materials, and significant improvements in the properties are often associated with the development of novel microstructures. In this regard, eutectic crystals grown from the melt constitute a family of in-situ composites with a very fine microstructure and excellent bonding between the phases. If they are produced by directional solidification, the small phase size together with the absence of grain boundaries in the transverse direction hinders the presence of defects and significantly increases the mechanical properties of brittle ceramic eutectics [1,2]. In addition, the phases in the eutectic are thermodynamically compatible up to temperatures approaching the eutectic temperature, which opens great possibilities for high-temperature applications, particularly in the case of eutectic ceramic oxides, where each

phase is also chemically stable in oxidizing environments even at very high temperatures.

Among the different eutectic ceramic oxides, the $\text{Al}_2\text{O}_3\text{--ZrO}_2(\text{Y}_2\text{O}_3)$ system is one of the most interesting materials from the point of view of its mechanical properties as well as its strength retention at high temperature. The flexure strength at ambient temperature of the first $\text{Al}_2\text{O}_3\text{--ZrO}_2(\text{Y}_2\text{O}_3)$ eutectics manufactured in the 1970s and 1980s was modest (< 600 MPa) [3,4], but this strength was retained up to 1850 K, at which flexure strength values of up to 524 MPa were measured [3]. Significant improvements in the processing techniques in the last decade have demonstrated that ambient temperature strengths in the range 1.0–1.5 GPa can be obtained by carefully controlling the microstructure [5–8]. However, the mechanical properties at high temperature of these novel microstructures were only analyzed by Sayir et al. [9]. They found that the strength of the eutectic fibers decreased from 1.2 GPa at room temperature to approximately 800 MPa at 1673 K, but the mechanisms responsible for this behavior were not studied in detail. It is evident that further improvements in the mechanical properties in these eutectic ceramic oxides at ambient and elevated temper-

* Corresponding author. Tel.: +34-913-365375; fax: +34-915-437845.

E-mail address: jllorca@mater.upm.es (J. LLorca).

ature require a deeper knowledge of the deformation and failure micromechanisms as a function of the temperature and microstructure. This was the main aim of this investigation.

2. Processing and experimental techniques

The $\text{Al}_2\text{O}_3\text{-ZrO}_2(\text{Y}_2\text{O}_3)$ eutectics were prepared from a powder mixture of 34.5 mol% of ZrO_2 (Alfa 99% purity), 3.5 mol% of Y_2O_3 (Aldrich 99.99%) and 62 mol% of Al_2O_3 (Aldrich 99.99%), which was pressureless sintered at 1500°C to obtain precursor rods. The commercial Al_2O_3 powders presented traces of Cr. These traces were enough to carry out the piezospectroscopic studies described below without further doping. Directionally solidified eutectic rods of 50–100 mm in length were grown at 30 mm/h from the precursor rods by the laser-heated float zone method, as described elsewhere [10,11]. The rod diameter was 1.3–2.2 mm, depending on the diameter of the precursor rod.

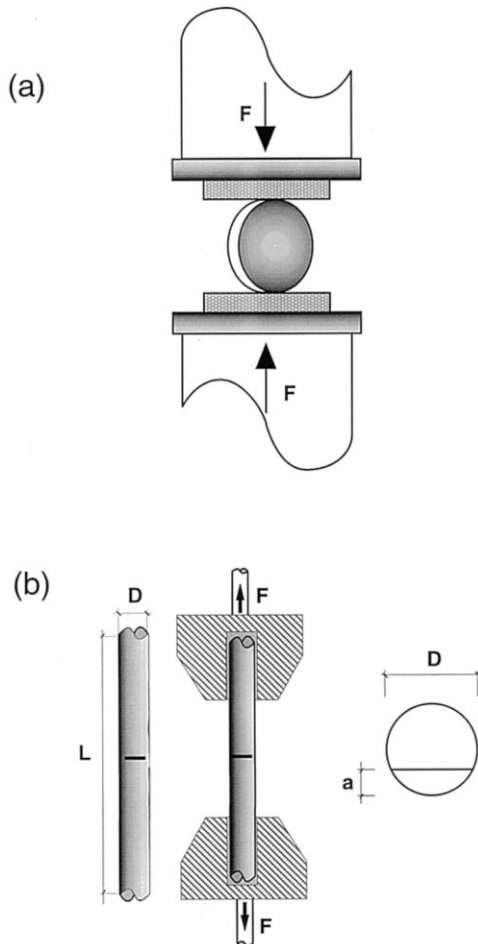


Fig. 1. Experimental set-up. (a) Diametral compression test. (b) Fracture test.

Longitudinal and transversal sections were cut from the rods using a diamond saw, and initially polished using diamond of $30\ \mu\text{m}$ grain size as abrasive, and afterwards with a diamond slurry (up to $1\ \mu\text{m}$). The polished surfaces were first cleaned in deionized water, and subsequently by ultrasound in butanone and ethanol. The surfaces were coated with a thin layer of Au–Pd, and the microstructure was observed in a Jeol-jsm-6300 scanning electron microscope equipped with energy-dispersive X-ray microanalysis. Secondary and back-scattered electron detectors were used to ascertain the particular characteristics of the microstructure along the rod and across the diameter.

The dynamic elastic modulus of the rods in the longitudinal direction was determined by the flexural vibration resonance method on fibers of 30 mm in length (Grindosonic MK4i, J.W. Lemmens, Belgium). In addition, the Vickers hardness was measured with a microhardness tester (Akashi MVK-E II) on polished longitudinal and transverse sections of the rods at a load of 98 N.

The flexure strength of the rods in the longitudinal direction from 300 to 1700 K was measured through flexure tests carried out in a ceramic three-point bend testing fixture with 6 mm loading span. The specimen and the loading fixture were placed in a furnace and loaded through two alumina rods connected to the actuator and load cell, respectively, of a servo-mechanical testing machine. The heating rate was $18\ \text{K min}^{-1}$ up to 1073 K, $8\ \text{K min}^{-1}$ up to 1473 K, and $5\ \text{K min}^{-1}$ above this point. The specimen was held at the test temperature for 30 min before testing. All the tests were performed in air under stroke control at a cross-head speed of $10\ \mu\text{m min}^{-1}$. The flexure strength was computed from the maximum load in the test according to the Strength of Materials theory for an elastic beam of circular section.

The transverse strength of the eutectic rods at 300 K was measured through the diametral compression test (also known as the Brazilian test), a standard procedure to measure the tensile strength of concrete [12] and other ceramic materials [13]. Circular disks of 1.2 mm in thickness were cut from the rods and subjected to diametral compression between two rigid ceramic plates (Fig. 1a). The tests were performed under stroke control at a cross-head speed of $12\ \mu\text{m min}^{-1}$. Assuming that the material is linearly elastic and that the contact area between the disk and the plates is very small (as compared to the disk diameter, D), the stress perpendicular to the compressed diameter, σ_t , is tensile and constant across the diameter. It is given by

$$\sigma_t = \frac{2F}{\pi DB} \quad (1)$$

where F is the compressive load and B the disc thickness. Although the compressive stresses in the load

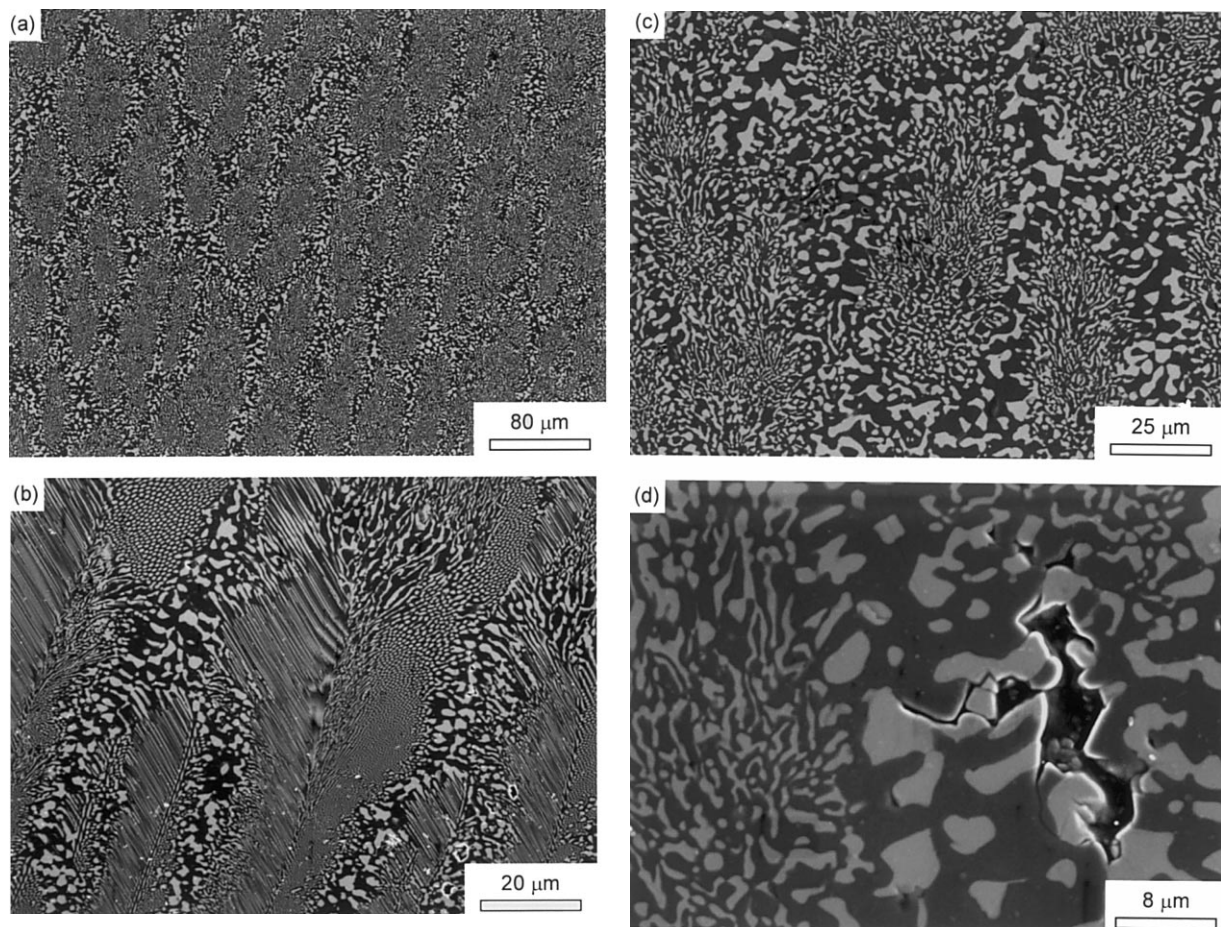


Fig. 2. Secondary electron micrographs showing the microstructure of the eutectic rods. (a) Longitudinal section of the rods. (b) Detail of the colony center showing the ordered ZrO_2 rods embedded in the Al_2O_3 matrix. (c) Detail of the colony center showing an interpenetrating network of both phases. (d) Longitudinal crack at the colony boundary. ZrO_2 appears white, and Al_2O_3 dark gray in the micrographs.

direction are much higher than the transverse tensile stresses, the disk fails by splitting across the compressed diameter in ceramic materials, where the compressive strength is significantly higher than the tensile strength.

The fracture toughness of the rods at 300 K was measured using two techniques. The first technique (Fig. 1b) was used in rods of 40 mm in length where a straight notch of depth $a = 0.34D$ was cut with a very thin diamond wire. The notch root radius was approximately 180 μm . The rod ends were introduced into cylindrical cavities machined in aluminum heads. The cavity diameter was 0.1 mm greater than that of the rods, which were glued to the aluminum using epoxy resin. The aluminum heads were connected to the actuator and to the load cell of the testing machine by nylon cords, providing a very flexible loading system, which ensured that the bending and torsional stresses on the rods were negligible. The notched rods were tested in tension until fracture under stroke control at a cross-head speed of 2 mm min^{-1} . The fracture toughness was computed from the failure load and the rod section using the appropriate expression for the stress

intensity factor [14]. The fracture toughness was determined also by the indentation fracture method, which relies on the cracks nucleated at the corners of the impressions made by the Vickers indenter during the hardness tests. The crack length was measured in the optical microscope, and the fracture toughness, K_{c} , was computed using the equation proposed by Niihara [15] for radial (Palmqvist) cracks from the indentation load (98 N), hardness and elastic modulus.

Finally, the broken samples were examined in the scanning electron microscope to determine the microstructural changes during high-temperature exposure and the associated failure mechanisms.

3. Eutectic microstructure

The analysis of the longitudinal sections showed that the microstructure of the rods was formed by colonies (Fig. 2a) consisting of a fine network of two phases, identified by Raman spectroscopy as tetragonal ZrO_2 (white) and $\alpha\text{-Al}_2\text{O}_3$ (dark gray) [11]. Under normal

conditions, cubic ZrO_2 is the stable phase for the nominal yttria/zirconia ratio in these samples. However, the Raman spectrum showed that most of the zirconia must be in the tetragonal form in our material. Although the Raman spectrum corresponding to tetragonal ZrO_2 can be better resolved than that of the cubic phase, our data suggest that the amount of cubic ZrO_2 , if any, is fairly in the minority with respect to the tetragonal phase [11].

The colony diameter in the transverse direction was $31 \pm 10 \mu\text{m}$, as measured by quantitative microscopy. The center of the colonies was formed by an ordered distribution of tetragonal ZrO_2 rods of approximately $0.3 \mu\text{m}$ in diameter (Fig. 2b), but a disordered interpenetrating network of both phases was sometimes prevalent (Fig. 2c). The colonies were elongated in the growth direction in the rod center, and their aspect ratio was around 3 (Fig. 2b and c). The colony aspect ratio and the inclination from the rod axis increased with the distance to the center due to the morphology of the solidification front, which forms a meniscus concave towards the solid phase. The colonies were surrounded by a thick boundary region ($13 \pm 4 \mu\text{m}$), which contained coarse ZrO_2 particles ($< 10 \mu\text{m}$). Pores and cracks oriented in the longitudinal direction were detected in this zone (Fig. 2d).

The longitudinal cracks at the colony boundaries were associated with decohesions at the $\text{ZrO}_2/\text{Al}_2\text{O}_3$ interfaces (Fig. 2d). Although the bonding between both phases was excellent, interface decohesion may be induced by the high thermal residual stresses developed upon cooling from the processing temperature as a result of the mismatch in thermal expansion coefficients between the phases. The magnitude of the average residual stresses in the alumina was obtained from the shift in position of the R_1 (14402 cm^{-1}) and R_2 (14432 cm^{-1}) intensity peaks in the luminescence spectra of Cr^{+3} in Al_2O_3 in the rods, as compared with that of unstressed ruby [11]. The shifts can be related to the average residual stresses in the longitudinal (growth axis, $\sigma_{//}$) and transverse (σ_{\perp}) directions using the piezospectroscopic tensors of the R-line emission determined by He and Clarke for ruby in compression [16]. These are shown in Table 1, together with the hydrostatic stress component, σ_h . The Al_2O_3 was subjected to compressive stresses within the eutectic composite, while the ZrO_2 was in tension. The magnitude of these stresses in ZrO_2 can be easily estimated through the

self-consistent method [11], and the corresponding values are also shown in Table 1. The large difference between the stresses in each phase has to be accommodated at the interface, and it is not surprising that cracks propagated from pores or small flaws upon cooling from the processing temperature. Of course, the longer cracks were likely to develop and grow at the colony boundaries, where the ZrO_2 grains were larger.

Approximate quantitative microscopy analysis indicated that the volume fractions of Al_2O_3 and ZrO_2 were, respectively, 70 and 30% in both types of microstructure. The crystallographic analysis of the regions with a colony microstructure was presented in a previous investigation [11] and agreed with the results reported by other authors in eutectics of similar composition also processed by directional solidification [17,18]. The alumina phase grew first from the melt as a continuous single crystal with the $\langle 0001 \rangle$ parallel to the growth direction. Examination of the microstructure using back-scattered electrons showed the presence of only two phases, Al_2O_3 and ZrO_2 (Fig. 3a). The scanning electron microscope images formed with the $K\alpha$ lines of Al (Fig. 3b), Zr (Fig. 3c) and Y (Fig. 3d) showed that the Y_2O_3 was completely dissolved into the ZrO_2 , and no segregation of yttria into the alumina or formation of yttrium-aluminum garnet was detected. No changes were observed in the microstructure after holding the samples for 1 h at 1700 K, and it was concluded that the microstructure of the rods was not affected by the heat treatment.

4. Mechanical behavior at ambient temperature

4.1. Elastic modulus

The average values of the flexural elastic modulus, E , the flexure strength, σ_f , the transverse tensile strength, σ_t , and the fracture toughness, K_{IC} , are shown in Table 2, together with the corresponding standard errors. The first interesting result in this table is the high value of the longitudinal elastic modulus, which is very close to the upper limit of 385 GPa predicted by the rule of mixtures from the volume fraction of each phase and their respective elastic moduli: 456 GPa in the $\langle 0001 \rangle$ direction for Al_2O_3 [19] and 220 GPa for tetragonal ZrO_2 [20]. This indicates that the cracks at the colony boundaries (Fig. 2d) were mainly oriented in the growth direction and barely affected the elastic properties in the longitudinal direction.

4.2. Longitudinal strength

The flexure strength of the $\text{Al}_2\text{O}_3\text{-ZrO}_2(\text{Y}_2\text{O}_3)$ rods was excellent. It was approximately 30–40% higher than that reported by Homeny and Nick [5] on eutec-

Table 1
Average values of the thermal residual stresses in Al_2O_3 and ZrO_2

	$\sigma_{//}$ (GPa)	σ_{\perp} (GPa)	σ_h (GPa)
Al_2O_3	-0.25	-0.42	-0.36
ZrO_2	0.84	0.95	0.91

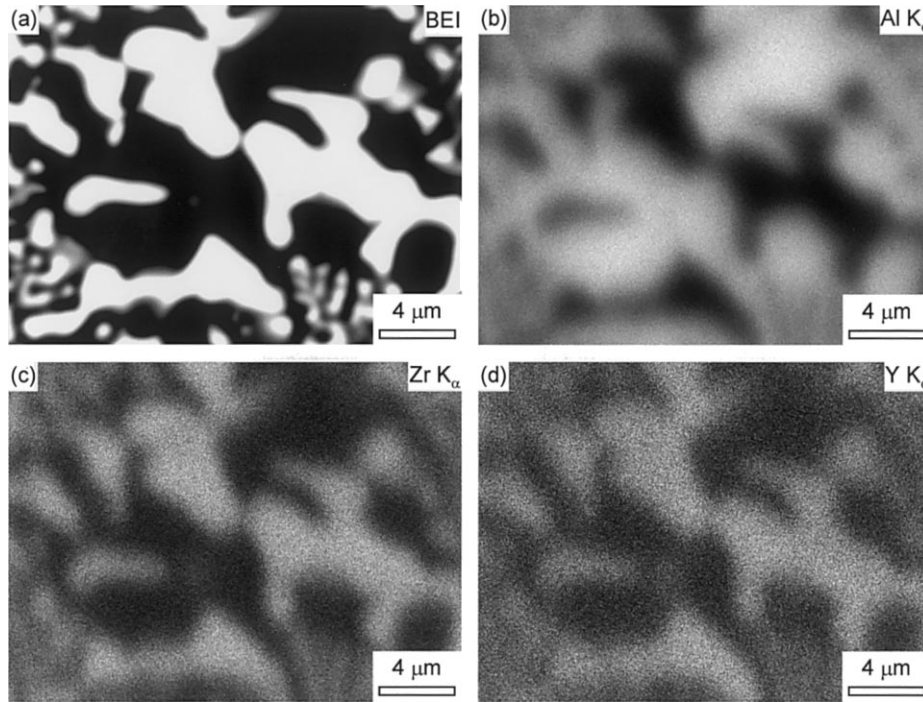


Fig. 3. Scanning electron microscope images obtained with: (a) back-scattered electrons, (b) K α lines of Al, (c) K α lines of Zr, (d) K α lines of Y.

tics processed by hot pressing and slightly lower than the results obtained by Bates [7] on fibers of 100–200 μm in diameter grown by the edge defined-film fed-growth method. The composition of this latter eutectic was practically equivalent to that of the rods studied here, and in addition, the microstructure of the material showed predominantly the colony structure shown in Fig. 2.

The study of the fracture surfaces in the scanning electron microscope showed that fracture was initiated in small defects located in the colony boundaries (Fig. 4), and the excellent strength of this eutectic composite arises as a combination of a fine microstructure and a high toughness. In a first approximation, it is sensible to assume that the surface defects leading to fracture behave as semicircular cracks, and their critical radius, a_c , can be computed as [21]

$$a_c = \frac{1}{\pi} \left[\frac{K_C}{0.65\sigma_f} \right]^2 = 36 \mu\text{m}. \quad (2)$$

This value is of the same order as the diameter of the colonies in Fig. 2a–c, whose size might be considered as the critical microstructural parameter controlling the flexure strength. In this regard, the combination of the experimental results of Bates [7] with those presented here seems to indicate that the flexure strength of the fibers increased as the colony size decreased (Fig. 5). It should be noted, however, that other authors found no increase in strength by reducing the colony size beyond a certain value [1]. They argued that the width of the

colony boundaries, as well as the porosity in these regions, increases as the colony diameter decreases. Thus, the width of the colony boundaries becomes the critical factor for small colony sizes, and no improvements in strength were observed when the average colony size was reduced beyond a certain value. The

Table 2
Mechanical properties of $\text{Al}_2\text{O}_3\text{-ZrO}_2(\text{Y}_2\text{O}_3)$ eutectics

E (GPa)	σ_f (MPa)	σ_t (MPa)	K_C (MPa \sqrt{m})
343 ± 7	1130 ± 50	80 ± 39	7.8 ± 0.3

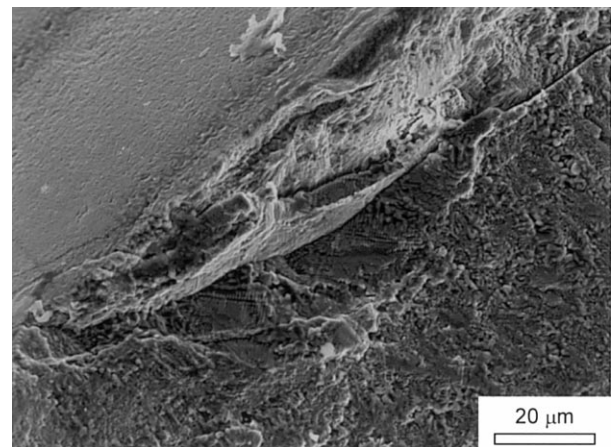


Fig. 4. Fracture initiating flaw at the surface of an $\text{Al}_2\text{O}_3\text{-ZrO}_2(\text{Y}_2\text{O}_3)$ rod tested in bending.

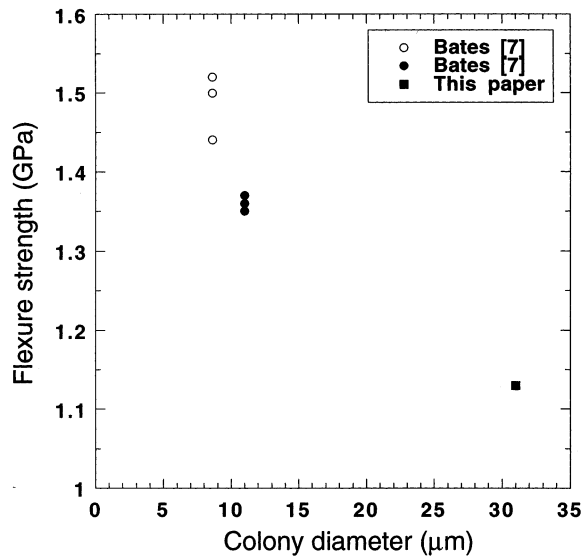


Fig. 5. Influence of colony size on the flexure strength of $\text{Al}_2\text{O}_3\text{-ZrO}_2(\text{Y}_2\text{O}_3)$ eutectics.

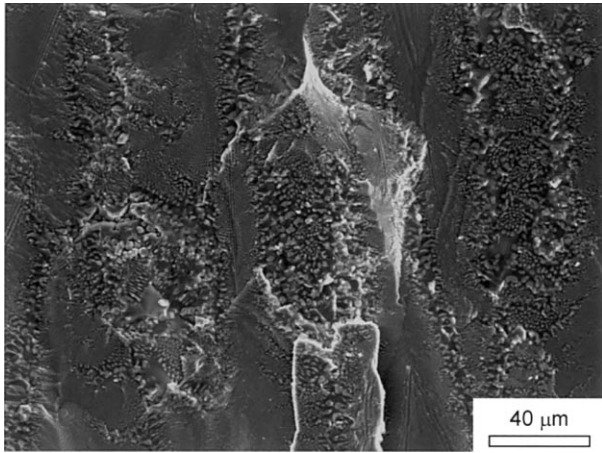


Fig. 6. Fracture surface of the samples broken in the diametral compression tests.

Table 3
Hardness and fracture toughness of $\text{Al}_2\text{O}_3\text{-ZrO}_2(\text{Y}_2\text{O}_3)$ eutectics

Orientation	Longitudinal	Transverse
H (GPa)	14.6 ± 0.1	15.3 ± 0.2
K_{c} (MPa $\sqrt{\text{m}}$)	5.2 ± 0.1	4.8 ± 0.1

maximum flexure strength of $\text{Al}_2\text{O}_3\text{-ZrO}_2(\text{Y}_2\text{O}_3)$ eutectics with a colony microstructure seems to be limited to ≈ 1.5 GPa (see Fig. 5), and higher strengths can only be achieved with different microstructures. These comments are in agreement with the results obtained by Farmer et al. [6], who measured flexure strengths of ≈ 2 GPa in fibers of the same composition and 100 μm in diameter processed by the edge-defined film-fed method. The fiber center was occupied by colonies of

12–15 μm in diameter, but the outer rim (which controlled the strength) was formed by a regular lamellar structure of up to 6 μm in depth made up of fine (0.1 μm) lamellae of both phases stacked alternately.

4.3. Transverse strength

The transverse strength of the rods at ambient temperature was characterized through six diametral compression tests. The results presented a large scatter, as shown in Table 2, where the average strength and the corresponding standard error are shown. The fracture surface of the samples tested in diametral compression presented an abrupt morphology, created by the intersection of various cracks propagated from the colony boundary defects (Fig. 6). The fracture stress depended on the size and orientation of these critical defects, and this caused the large scatter in the results among the different samples.

The large difference between the longitudinal and the transverse strength for the colony microstructure is worth noting. As shown below, this anisotropy cannot be attributed to the differences in crack propagation resistance between longitudinal and transverse directions but was mainly induced by the presence of elongated cracks in the boundary colonies oriented in the growth direction.

4.4. Fracture toughness

As well as being due to a fine microstructure, the high strength of the $\text{Al}_2\text{O}_3\text{-ZrO}_2(\text{Y}_2\text{O}_3)$ eutectic was also due to the high fracture toughness of the material. This was previously reported by other authors, who measured the toughness of this eutectic by the indentation fracture method [5,22], but no justification of the high toughness of these eutectic composites has yet been provided. The interaction between the microstructural features and the cracks nucleated from the corners of Vickers indentations was analyzed in the scanning electron microscope, and these tests provide new values for the composite toughness as well as for the hardness in the longitudinal and transverse directions. The average values, obtained from approximately 10 indentations for each orientation, are presented in Table 3, together with the corresponding standard deviations.

The hardness values were very high and similar to those measured by Echigoya et al. [22]. In addition, well-defined cracks emerged from indentation corners (Fig. 7a), and it was possible to estimate the fracture toughness in the longitudinal and transverse directions (Table 3). In agreement with Ref. [22], these results indicated that the fracture resistance was only marginally higher in the transverse direction, and the toughness of this directionally solidified eutectic could be considered isotropic. Thus, the difference between

the longitudinal and transverse strength was due to the orientation of the defects in the microstructure and not to any variation of the crack propagation resistance with orientation. Evidently, the orientation of the defects was induced by the directional solidifi-

cation process, which generated colonies elongated along the growth axis.

It should be noted at this point that the toughness values obtained with this technique are a crude approximation to its ‘true’ magnitude, because they depend on a number of factors (mainly the actual shape of the cracks and the residual stresses), which cannot be controlled accurately during the test. Nevertheless, they showed that the toughness of the eutectic oxide was significantly higher than that of each phase separately, in agreement with the fracture tests presented in Section 4.2, and indicated the presence of additional energy dissipation mechanisms responsible for this behavior. In addition, the results in Table 3 can be compared directly with those obtained through the same technique in $\text{Al}_2\text{O}_3\text{--Y}_3\text{Al}_5\text{O}_{12}$ (2.0–2.4 MPa \sqrt{m}) [23] or $\text{Al}_2\text{O}_3\text{--Gd}_2\text{O}_3$ (5–6 MPa \sqrt{m}) [24], which indicate that $\text{Al}_2\text{O}_3\text{--ZrO}_2(\text{Y}_2\text{O}_3)$ eutectics stand among the toughest directionally solidified eutectic oxides.

The analysis of the crack path in the scanning electron microscope showed a mixture of transgranular and intergranular fracture, where the former was dominant. It was also observed that several cracks often emerged from the corner of the Vickers indentation (Fig. 7a and b) and propagated in parallel for a certain distance until one of them became dominant and the others were arrested. In general, crack arrest followed by the development of another parallel crack a few microns above or below the first crack tip was observed throughout the crack path. This led to the development of elastic bridges behind the main crack tip during crack propagation, as shown in Fig. 7c. It is well known (see, for instance, Ref. [25]) that both crack overlapping and bridging in the crack wake are effective toughening mechanisms in brittle solids and were responsible for the high toughness of the eutectic composite.

The high fracture resistance of the eutectic oxide cannot be attributed to the stress-induced tetragonal to monoclinic transformation in the ZrO_2 because the amount of Y_2O_3 in solid solution (≈ 10 mol%) stabilizes completely the tetragonal phase. More likely, the crack pattern detected in Fig. 7 is indicative of the coexistence of phases and interfaces with different crack-growth resistance, which, together with the thermal residual stresses, lead to crack deflection, branching and, ultimately, the development of elastic ligaments in the crack wake. However, the analysis of the fracture surfaces could not reveal the role of each phase of the $\text{Al}_2\text{O}_3\text{--ZrO}_2$ interface and of the residual stresses during crack propagation. The crack was arrested sometimes in either phase and propagated preferentially through the interface in other situations, but no clear pattern could be established.

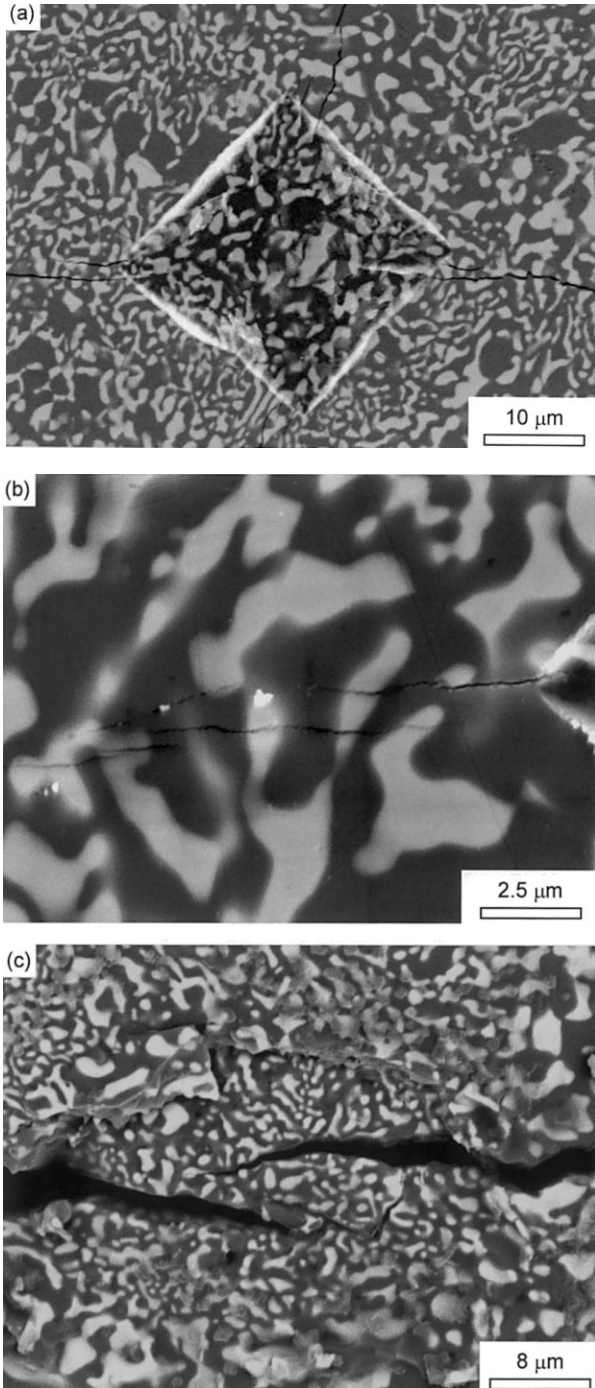


Fig. 7. Fracture micromechanisms in $\text{Al}_2\text{O}_3\text{--ZrO}_2(\text{Y}_2\text{O}_3)$ eutectics. (a) Cracks emerging from the corner of a Vickers indentation in the colony regions. (b) Multiple cracks nucleated near the tip of Vickers indentation. (c) Back-scattered electron image of an elastic ligament between the crack surfaces in the crack wake.

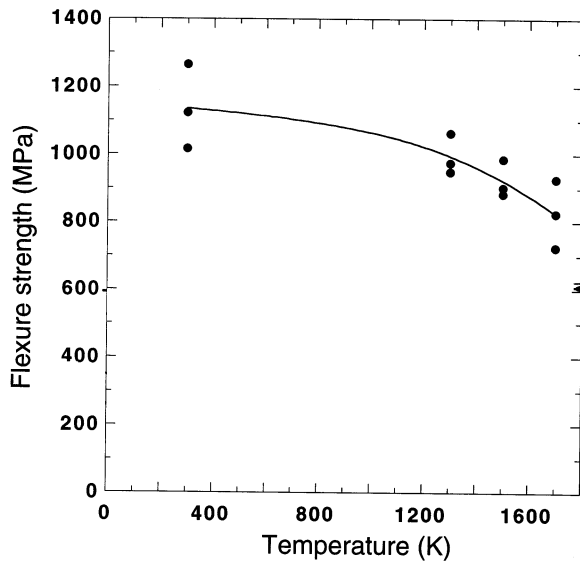


Fig. 8. Influence of the temperature on the longitudinal flexure strength of $\text{Al}_2\text{O}_3\text{-ZrO}_2(\text{Y}_2\text{O}_3)$ eutectics.

5. Flexure strength at high temperature

The effect of the temperature on the longitudinal strength of the $\text{Al}_2\text{O}_3\text{-ZrO}_2(\text{Y}_2\text{O}_3)$ eutectics was ascertained through three-point bending tests at 300, 1300, 1500, and 1700 K. At least three tests were carried out at each temperature, and the results are plotted in Fig. 8. Regardless of the experimental scatter, they are in agreement with the behavior reported by Sayir et al. [9], who also measured flexure strengths of the order of 800 MPa at 1673 K. It is worth noting that this strength is rather higher than that measured either in monolithic ceramics (Si_3N_4 , SiC) or in whisker- and fiber-reinforced ceramic composites at the same temperature [26]. The strength drops rapidly in monolithic and whisker-reinforced materials above 1300 K due to the softening of the glassy phases at the grain boundaries, while fiber and interface degradation severely reduce the properties of fiber-reinforced ceramics above 1500 K [27,28].

The loading-curve tests did not show any evidence of non-linear deformation before fracture even at a high temperature, and failure occurred catastrophically when a crack began to propagate from a surface defect. Examination of the fracture surfaces in the scanning electron microscope showed that the critical crack was nucleated at surface defects associated with decohesions at the colony boundaries. They could not be distinguished from those observed at ambient temperature (Fig. 4) and for the sake of brevity are not plotted here. In addition, no evidence of plastic deformation was found in the analysis of the fracture surfaces. These observations indicate that exposure to temperatures as high as 1700 K for short periods of time (less than 1 h in all cases) did not lead to the nucleation of new

defects in the microstructure and was not the cause of the strength reduction. Farmer et al. [6] reached the same conclusion in $\text{Al}_2\text{O}_3\text{-ZrO}_2(\text{Y}_2\text{O}_3)$ eutectic processed by the laser-heated float zone method. The average bending strength of the fibers did not change after annealing for 4 h at 1673 K. It should be noted, however, that annealing for 196 h at 1673 K did reduce the flexure strength from ≈ 1 to ≈ 0.7 GPa. Fracture in the annealed samples in this latter case originated in regions of exaggerated coarsening of the eutectic structure.

Mah et al. [29] found that the flexure strength in $\text{Al}_2\text{O}_3\text{-Y}_3\text{Al}_5\text{O}_{12}$ eutectic rods (≈ 10 mm in diameter) produced by the modified Bridgman method dropped from 373 MPa at 300 K to 272 MPa at 1648 K. As in our $\text{Al}_2\text{O}_3\text{-ZrO}_2(\text{Y}_2\text{O}_3)$ eutectic rods, no changes in the microstructure were observed. The evolution of the flexure strength with temperature was mainly due to the reduction in the fracture toughness, which could be measured at both temperatures owing to the larger diameter of the samples. The small diameter of our eutectic rods impeded fracture testing at high temperature, but the evidence from the fractographic analysis indicates that the reduction in the flexure with temperature could be attributed to a proportional decrease in the fracture toughness. Even though, the toughness of the eutectic rods at 1700 K — estimated through Eq. (2) — should be around $5.7 \text{ MPa} \sqrt{m}$, significantly higher than that of either alumina or zirconia at this temperature. This behavior can be rationalized in terms of the same mechanisms as those proposed at ambient temperature: the differences in the crack growth resistance of both phases and of the interface lead to crack deflection and branching and, ultimately, to the development of elastic bridges in the crack wake. The progressive reduction in the eutectic toughness as a function of temperature was due to the release of the thermal residual stresses that enhance these toughening micromechanisms.

6. Concluding remarks

$\text{Al}_2\text{O}_3\text{-ZrO}_2(\text{Y}_2\text{O}_3)$ rods were produced by directional solidification using the laser-heated float zone method. The microstructure of the eutectic oxides was mainly formed by colonies consisting of a fine network of ZrO_2 and $\alpha\text{-Al}_2\text{O}_3$. The colonies (transverse diameter $\approx 31 \pm 10 \mu\text{m}$) were elongated in the growth direction and were surrounded by a thick boundary region (thickness $\approx 13 \pm 4 \mu\text{m}$) which contained pores and cracks oriented in the longitudinal direction.

The mechanical properties of the rods in the longitudinal direction were excellent, with a flexure modulus of 343 GPa and an average flexure strength over 1.1 GPa. The excellent strength was a result of the combination

of the high toughness of the eutectic rod ($7.8 \text{ MPa} \sqrt{m}$) with a small critical defect size. This was demonstrated by the fractographic analysis, which showed that fracture was initiated in surface defects associated with pores and longitudinal cracks at the colony boundaries. The area of these defects was much larger perpendicularly to the transverse direction, and thus the transverse tensile strength decreased in more than one order of magnitude.

The analysis of the crack profile often showed two or more microcracks propagating in parallel for a certain distance until one of them became dominant and the others were arrested. This led to the development of elastic bridges behind the crack tip, and both crack overlapping and bridging in the crack wake were responsible for the high toughness of the eutectic composite. It is believed that the coexistence of phases and interfaces with different crack growth resistance, together with the thermal residual stresses, was responsible for the deflection and branching of the crack during propagation.

Finally, the excellent mechanical properties in the longitudinal direction were maintained up to 1700 K, where average flexure strengths in excess of 800 MPa were measured. This behavior is significantly better than that of either monolithic ceramics (Si_3N_4 , SiC) or whisker- and fiber-reinforced ceramic composites at the same temperature. It was shown that the eutectic microstructure was stable after 1 h at 1700 K, and the origin of the strength reduction was very likely associated with the drop in the eutectic oxide toughness caused by the release of the thermal residual stresses.

Acknowledgements

The financial support from CICYT through grants MAT97-672-C02-01 and 02 is gratefully acknowledged.

References

- [1] V.S. Stubican, R.C. Bradt, *Ann. Rev. Mater. Sci.* 11 (1991) 267.
- [2] R.L. Ashbrook, *J. Am. Ceram. Soc.* 60 (1976) 428.
- [3] C.O. Hulse, J.A. Batt, *Effects of Eutectic Microstructures on the Mechanical Properties of Ceramic Oxides*. Report UARL N910803, 1974, p. 140.
- [4] V.A. Borodin, M.Y. Starostin, T.N. Yalovets, *J. Crystal Growth* 104 (1990) 148.
- [5] J. Homeny, J.J. Nick, *Mater. Sci. Eng.* A127 (1990) 123.
- [6] S.C. Farmer, A. Sayir, P.O. Dickerson, *In situ Composites, Science and Technology*, TMS, Warrendale, PA, 1993, pp. 167–182.
- [7] H.E. Bates, *Ceram. Eng. Sci. Proc.* 13 (7/8) (1992) 190.
- [8] E.L. Courtright, J.S. Haggerty, J. Sigalovsky, *Ceram. Eng. Sci. Proc.* 14 (7/8) (1993) 671.
- [9] A. Sayir, S.C. Farmer, P.O. Dickerson, H.M. Yun, *Mater. Res. Soc. Symp. Proc.*, vol. 365, MRS, Warrendale, PA, 1995, pp. 21–27.
- [10] J.I. Peña, R.I. Merino, G.F. de la Fuente, V.M. Orera, *Adv. Mater.* 8 (1996) 909.
- [11] J.A. Pardo, R.I. Merino, V.M. Orera, J.I. Peña, C. González, J.Y. Pastor, J. LLorca, *J. Am. Ceram. Soc.*, 83 (2000) 2745.
- [12] *Standard Test Method for Splitting Tensile Strength of Cylindrical Concrete Specimens, C496-90*. Annual Book of ASTM Standards, vol. 04.02, American Society for Testing and Materials, Philadelphia, PA, 1991.
- [13] J.Y. Pastor, P. Poza, J. LLorca, *J. Am. Ceram. Soc.* 82 (1999) 3139.
- [14] A. Levan, J. Royer, *Int. J. Fract.* 61 (1993) 71.
- [15] K. Niihara, R. Morena, D.P.H. Hasselman, *J. Mater. Sci. Lett.* 1 (1982) 13.
- [16] J. He, D.R. Clarke, *J. Am. Ceram. Soc.* 78 (1995) 1347.
- [17] L. Mazerolles, D. Michel, R. Portier, *J. Am. Ceram. Soc.* 69 (1986) 252.
- [18] M. Yu, B.A. Starostin, T.N. Yalovets, *J. Crystal Growth* 171 (1997) 119.
- [19] W.J. Tropf, M.E. Thomas, T.J. Harris, *Handbook of Properties of Crystals and Glasses*, McGraw-Hill, New York, 1995.
- [20] E.C. Subbarao, in: A.H. Heuer, L.W. Hobbs (Eds.), *Science and Technology of Zirconia*, vol. 3, The American Ceramic Society, Westerville, OH, 1981, pp. 1–24.
- [21] J.C. Newman, I.S. Raju, *Eng. Fract. Mech.* 15 (1981) 185.
- [22] J. Echigoya, Y. Takabayashi, H. Suto, *J. Mater. Sci. Lett.* 5 (1986) 153.
- [23] J.-M. Yang, S.M. Seng, S. Chang, *J. Am. Ceram. Soc.* 79 (1996) 1218.
- [24] Y. Waku, N. Nakagawa, T. Wakamoto, H. Ohtsubo, K. Shimizu, Y. Kohtoku, *Nature* 389 (1997) 49.
- [25] B. Lawn, *Fracture of Brittle Solids*, Cambridge Solid State Science Series, Cambridge, 1993.
- [26] J.-M. Yang, T.N. Tieg, in: S.V. Nair, K. Jakus (Eds.), *High Temperature Mechanical Behavior of Ceramic Composites*, Butterworth-Heinemann, Boston, MA, 1995, pp. 87–119.
- [27] J. LLorca, M. Elices, J.A. Celemin, *Acta Mater.* 46 (1998) 2441.
- [28] J.A. Celemin, J. LLorca, *Comp. Sci. Technol.* 60 (2000) 1067.
- [29] T. Mah, T.A. Parthasarathy, L.E. Matson, *Ceram. Eng. Sci. Proc.* 11 (1990) 1617.